# Unveiling the conformational diversity of succinic acid: Insights from IR spectroscopy and quantum chemical calculations

Lucas da Silva Sa, Ander Camiruaga, Katia Le Barbu-Debus, Jordan Claus, Manuel Goubet, Rodolphe Pollet, Wutharath Chin

# Unveiling the conformational diversity of succinic acid: Insights from IR spectroscopy and quantum chemical calculations

Lucas Da Silva Sa,[1] Ander Camiruaga,[1, a)] Katia Le Barbu-Debus,[1] Jordan A. Claus,[2, b)] Manuel Goubet,[2] Rodolphe Pollet,[3] and Wutharath Chin[1]

[1)] *Université Paris-Saclay, CNRS, Institut des Sciences Moléculaires d'Orsay, 91405, Orsay, France*

[2)] *University of Lille, CNRS, UMR 8523-PhLAM, Physique des Lasers, Atomes et Molécules, F-59000 Lille, France*

[3)] *Université Paris-Saclay, CEA, CNRS, NIMBE, 91191, Gif-sur-Yvette, France*

(*Electronic mail: wutharath.chin@universite-paris-saclay.fr.)

Small $\alpha$-dicarbonyl compounds like succinic acid are found abundantly in the atmosphere, thereby contributing to the formation of secondary organic aerosols through solid or liquid particles and gas-phase molecular clusters. The vibrational spectrum of succinic acid was measured in two different environments to evidence the role of the medium on the geometry adopted by the acid. Different structures were observed. The planar and extended structures of succinic acid were favored in the solid state whereas the non-planar gauche conformer was the predominant form in an argon matrix at 20K, similar to the gas phase. Aided by quantum chemistry calculations and the NCI analysis we investigated the conformational diversity of succinic acid to understand the factors that govern the stability of the acid.

## I. INTRODUCTION

Small $\alpha$-dicarbonyl compounds such as succinic acid are abundant pollutants in the atmosphere[1,2]. They are present in solid or liquid particles and as such, they likely contribute to the formation of secondary organic aerosols[3–5]. Because they can also form gas-phase molecular clusters they are considered good candidates for forming pre-nucleation clusters implied in the so-called new particle formation[4,6–8]. For instance, succinic and citric acids have been found as the most abundant acids in remote areas such as Antartica[2]. Succinic acid is a secondary product of the oxidation of organic precursors present in sea-sprayed aerosols, such as isoprene, and unsaturated fatty acids. There have been extensive investigations on the solid-phase structure of succinic acid. The $\beta$-form is the most stable crystalline structure at ambient conditions[9–15], adopting a monoclinic structure. The structure is modified at higher temperatures above 137°C towards the $\alpha$-polymorph crystal structure with a triclinic symmetry[12]. In the two polymorphic states, succinic acid displays a dimer-like geometry where the acidic groups face each other forming intermolecular hydrogen bonds[11,13–15].

Results are scarcer in the gas phase because of the loss of water when bringing succinic acid in the gas phase, thereby readily converting to its anhydride form[16,17]. The clustering of succinic acid with atmospheric nucleating precursors was investigated theoretically, but there has been no experimental counterpart[18]. Two structural studies based on electron diffraction and rotational spectroscopy and guided by extensive quantum chemistry calculations were devoted to gas-phase succinic acid. The most stable form was reported to adopt a *gauche* conformation[19] being stabilized by the so-called *gauche* or *methylene effect*[20]. The extended planar geometry that was evidenced in the solid phase could not be observed by rotational spectroscopy because of the absence of a permanent dipole moment in this conformation. Conversely, a mixture of four conformers having *gauche* and *anti* configuration was evidenced by electron diffraction, and the *gauche* forms were found to be predominant[19].

Studies in solution highlighted the co-existence of different forms of succinic acid. The protonated form can coexist with the monovalent succinate anion and the divalent succinate ion[21,22]. The ionic species were found to be predominant in bulk water, but the protonated form predominated at the air/water interface[22,23]. The extended-like structures of succinic acid predominated near the surface and in bulk solution at low concentrations, whereas the *gauche* species were favored at higher concentrations. The results were rationalized in terms of solvation propensity, representing the higher availability of the carboxyl groups for hydrogen bonding with water in the bulk. That the extended-like conformers were dominant near the surface was explained by their planar conformation and the coplanar orientation they adopt towards the air/water interface, namely, they are more "parallel" with the interface than the *gauche* forms.

Matrix isolation spectroscopy is a condensed-phase technique. However, it is well known that the species trapped in the matrix do not adopt typical liquid-phase conformations, but those encountered in the gas phase. Therefore, this technique enables us to catch the intrinsic properties of succinic acid without suffering from technical issues related to low dipole moments or packed interactions, or without discarding the delicate question of solvation effects on the conformation as is often the case in aqueous solution[24]. Because the structural landscape of succinic acid is complex and is influenced by its environment, it may still be an open question. We thus decided to investigate further its conformational diversity relying on IR spectroscopy coupled with matrix isolation, aided by theoretical methods. It is crucial for a better understanding of the role of geometry on acid aggregation that is the prior

[a)] present address: University of the Basque Country, Bilbao, Spain.

[b)] present address: Dipartimento di Chimica "Giacomo Ciamician", Universita di Bologna, 40126 Bologna, Italy.

step to pre-nucleation.

## II. EXPERIMENTAL METHODS

Succinic acid was purchased from Sigma Aldrich (>98%) and used without further purification. The IR absorption spectra of succinic acid were measured in the mid-IR domain (4000 - 1000 $cm^{-1}$) by FTIR spectroscopy to yield the vibrational signature, hence the structure of the succinic acid conformers present in the sample. The spectra in two different environments were compared, i.e. in a potassium bromide (KBr) pellet and argon matrices at cryogenic temperatures. The IR spectra were measured with a Thermofisher iS-50 FTIR spectrometer equipped with a Globar light source and a KBr beamsplitter and purged with dry air. The internal DTGS and the external MCT detectors were used for the measurements in KBr pellet and solid argon, respectively.

### A. Solid state studies

Succinic acid was mixed with potassium bromide (KBr) powder in a 1:1000 mass ratio. The pellet was put in the hole of an in-house plate, which was directly put in the FTIR spectrometer. No optical window was used during the IR acquisition. The IR spectra were obtained by accumulating 10 scans at a 1 $cm^{-1}$ resolution. All spectra in KBr are presented in an absorption mode, namely as positive bands, as obtained from Beer-Lambert's law. Blank spectra consisted of acquisitions with no sample.

### B. Matrix isolation

The setup was described previously[25]. We only briefly present it here. The cryogenic samples were obtained by flowing argon (Ar) gas above the succinic acid reservoir heated to 355 K. The mixture was then deposited onto a $BaF_2$ window kept at 20 K in a Displex closed-cycle cryostat where it condensed into a nearly crystalline solid. The setup used did not allow for a precise estimation of the absolute concentration of succinic acid. A rough estimate for the succinic acid/Ar ratio is 2/1000. The IR spectra were measured at 0.5 $cm^{-1}$ resolution in the mid-IR 600 - 4000 $cm^{-1}$ spectral region by accumulating 500 scans. In some samples, there were traces of water and succinic anhydride. The presence of the anhydride is due to the thermal degradation of succinic acid during the heating of the powder. The vapor pressure of succinic acid being quite low, the production of the anhydride is easily obtained even at low heating temperatures. We removed the contribution of the anhydride by recording a sample of succinic anhydride isolated in argon and subtracting its contribution from the spectrum of succinic acid. Hence, the IR bands discussed hereafter belong to the sole succinic acid species.

## III. COMPUTATIONAL METHODS

We employed different approaches to analyzing the conformational landscape of succinic acid, namely conformational searching, geometry optimization, frequency calculations with quantum chemistry, and topological analysis of the non-covalent interactions.

### A. Conformational search

We performed a conformational search using the iMTD-GC sampling algorithm[26] based on metadynamics simulations[27] at the GFN2-xTB level of theory[28] implemented in the CREST software[26] to identify the first set of relevant conformations for succinic acid. The latter were geometry optimized with quantum chemistry calculations at the HF/6-311++G(d,p) level of theory. A new set of 30 structures was obtained within an energy window of 50 kJ $mol^{-1}$ and each structure was optimized using DFT with the B3LYP functional, and post-Hartree Fock MP2 method with the 6-311++G(d,p) basis set. The D3BJ Grimme correction was employed to allow for a better description of the dispersion forces[29]. The harmonic IR frequencies were computed on the optimized geometries with the same methods. All calculations were run with the Gaussian(R) 16 suite of programs[30]. Post-processing of the outputs employed Visual Molecular Dynamics (VMD)[31,32] and Gabedit[33].

The calculations yield gas-phase vibrational frequencies in the harmonic approximation. We used scaling factors to correct (i) the anharmonicity, and (ii) the effect of the environment, KBr or argon matrix, that induces a spectral shift compared to the gas-phase values. The scaling factors differed depending on i) KBr or argon environment and ii) the spectral region.We used the following scaling factors for solid-state experiments because they that gave the best accord with the recorded spectrum in KBr: 0.905 for the OH stretch, 0.96 from 1800 to 1200 $cm^{-1}$, 0.94 below 1200 $cm^{-1}$. The scaling factors used for comparison with the argon matrix results were rather standard[34,35]: 0.975 in the fingerprint region (1800 - 800 $cm^{-1}$), and 0.945 in the OH stretch region (3800 - 3200 $cm^{-1}$). The electronic energies were calculated and corrected for zero-point energies. Unless mentioned, all energy values refer to relative electronic energies from the most stable conformer calculated at the B3LYP-D3BJ level of theory and are given in kJ/mol.

### B. Non-covalent interactions - NCI

The analysis of the non-covalent interactions relied on the topological analysis of the electronic density function using the NCI approach, as implemented in NCIPlot[36,37]. The reduced density gradient $s(\rho)$ and the eigenvalue of the Hessian of the electron density $\lambda_2$ were calculated using the optimized geometries at the B3LYP-D3BJ and MP2 levels of theory, as defined by:

$$s(\rho) = \frac{1}{2(3\pi^2)^{1/3}} \frac{|\nabla\rho|}{\rho^{4/3}}$$

Domains of weak electron density and low reduced density gradient $s(\rho)$ correspond to interatomic close contacts. This approach is well-suited for interactions such as hydrogen bonds or van der Waals interactions. The 2D NCI graphs plot the reduced gradient $s(\rho)$ as a function of the electron density $\rho$ times the sign of $\lambda_2$ in regions of low reduced gradient. The sign of $\lambda_2$ tells about the bonding ($\lambda_2 < 0$) or the nonbonding ($\lambda_2 > 0$) character of the interaction. Points of space of low reduced gradient $s(\rho)$ relating to these close contacts are visualized by 3D isosurfaces ($s(\rho)$=0.6 typically). The color code of the 3D-isosurfaces correlates with the interaction strength: blue indicates strong attractive interactions, green color indicates weak attractive interactions, and red refers to repulsive interactions. We used a custom Python script to create the reduced density gradient 2D plots and we used the VMD software for visualizing the 3D isosurfaces. The NCI plot of one specific conformer was drawn as a one-color graph for ease of comparison between two different forms of succinic acid.

## IV. RESULTS AND DISCUSSION

This section presents the effect of the environment on the succinic acid structure. The conformational landscape of succinic acid is discussed based on the conformers' vibrational signature aided by computational studies. We analyze the theoretical results first, then the experimental IR spectra.

### A. Structures and energetics

The 30 structures evidenced by the conformational search procedure (molecular dynamics and HF preliminary optimization) were re-optimized at the DFT and MP2 level of theory. 24 structures were found to be real minima with no imaginary frequencies. We found four non-equivalent conformers (namely *tt-Aaa*, *tt-Agg*, *tc-Aaa*, *cc-Aaa*) and ten pairs of isoenergetic mirror images (*tt-Gaa*, *tt-Gga*, *tt-Aga*, *tt-Ggg*, *tt-Agg*, *tc-Gag*, *tc-Gga*, *tc-Ggg*, *tc-Aga*, and *cc-Gag*) – see next section for the nomenclature. The carboxyl groups were planar in all conformers, with less than 5° deviation.

#### 1. Nomenclature

Succinic acid is very flexible due to torsions around the single bonds. We built on the labeling used in Ref.[19,23] for the description of the conformers. The following terminology is used to account for this large flexibility and identify the different conformations:

1. *A* and *G*, respectively *anti* and *gauche* refer to the $C_1CC'C_2$ dihedral angle of the carbon skeleton. *A* indicates a planar (or quasi planar) carbon backbone in an *anti* configuration (near 180°). Deviations of less than 20° are also considered as *anti*. *G* indicates a folded *gauche* carbon backbone with a dihedral angle of about ±60° or ±120°. We will refer to the *A* carbon backbone as linear conformers in the following.

2. The second and third letters *a* or *g* refer to the $O_1C_1CC'$ and $O_2C_2C'C$ dihedral angle, standing for *anti* and *gauche* configurations (respectively ±180°, and ±60°, with a deviation of ∼15°).

3. The prefixes *c* and *t*, for *cis* and *trans*, define the orientation of the carboxyl OH group with the carbon skeleton (HOCC dihedral angle of 0° and 180° respectively).

4. Ten conformers present symmetrical forms and are doubly degenerate (namely there are ten pairs of mirror conformers). They are marked with an asterisk. We will present only one form within the pair.

All structures are thus defined by a combination of three letters and a two-letter prefix. Two examples are given hereafter. The *tt-Aaa* conformation denotes a planar geometry where the central skeleton is *anti* (*A*), the two carboxyl groups are *anti* (*aa*) with the skeleton, and the OH groups are *trans* (*tt*-). The *tc-Gag* form denotes a folded carbon skeleton in a *gauche* (*G*) conformation, the *trans*-carboxyl group is *anti* (*a*) with the skeleton and the other *cis*-carboxyl group is in a *gauche* (*g*) orientation with the carbon backbone.

#### 2. Conformational landscape

The 24 structures have been grouped into three families according to the *cis* or *trans* orientation of the carboxyl group (see Figure 1). The most stable forms adopted a *tt* orientation, followed by the *tc* structures. The *cc* forms are the least stable. The relative energies of the conformers are given in Table I and the geometrical parameters are listed in Table S1 in the Supplementary Material (SM). *A* and *G* orientations, i.e. respectively linear and folded (or *gauche*) carbon backbone existed in each family. The structures are depicted in the Newmann-like projection for a clearer view of the backbone orientation in Figure S1 in SM.

We now describe the three families. The global minimum is the folded *tt-Gaa* structure whatever the level of theory used. It is similar to the conformer evidenced by gas-phase rotational spectroscopy[20]. In the *tt* family, 12 forms have been found to lie up to 14 kJ/mol above this most stable form. The second most stable conformer *tt-Aaa* at 2.0 kJ/mol adopts a completely planar geometry. The arrangement of the skeleton (capital letter *A* or *G*) seems to influence the energetic ordering since the lowest-lying *tt*-conformers alternatively adopt a *G/A/G/A/G/A* orientation. The *G*-conformer is indeed always more stable than the *A*-conformer, the other geometrical parameters being similar: **tt*-***G***aa is lower than *tt*-***A***aa, **tt*-***G***ga than **tt*-***A***ga, **tt*-***G***gg than **tt*-***A***gg (difference highlighted in bold). We also notice that the *anti*-orientation (i.e. label *a*)

TABLE I. Relative electronic energies corrected for zero-point energy $\Delta E$, relative Gibbs free energies $\Delta G$ at 298 K, and population p for the conformers of succinic acid obtained with B3LYP, B3LYP-D3BJ, and MP2 level of theory, with the 6-311++G(d,p) basis set (energies in kJ/mol, p in%).

| Conformer | B3LYP | | | B3LYP-D3BJ | | | MP2 | | |
|---|---|---|---|---|---|---|---|---|---|
| | $\Delta E$ | $\Delta G$ | p | $\Delta E$ | $\Delta G$ | p | $\Delta E$ | $\Delta G$ | p |
| **tt-Gaa* | 0.0 | 5.9 | 14.7 | 0.0 | 3.3 | 31.9 | 0.0 | 0.0 | 66.0 |
| *tt-Aaa* | 0.1 | 0.0 | 79.1 | 2.0 | 0.0 | 59.4 | 4.3 | 1.3 | 19.3 |
| **tt-Gga* | 6.0 | 11.9 | 1.3 | 5.7 | 9.2 | 2.8 | 5.0 | 5.9 | 6.0 |
| **tt-Aga* | 5.7 | 9.3 | 3.7 | 7.6 | 8.3 | 4.1 | 8.3 | 6.2 | 5.6 |
| **tt-Ggg* | 11.3 | 16.3 | 0.2 | 10.7 | 13.6 | 0.5 | 10.0 | 9.8 | 1.3 |
| **tc-Gag* | 13.5 | 22.2 | <0.1 | 11.9 | 17.7 | 0.1 | 17.3 | 19.4 | <0.1 |
| **tt-Ag$^-$g$^-$* | 11.1 | 14.3 | 0.5 | 12.8 | 13.0 | 0.6 | 12.3 | 10.2 | 1 |
| *tt-Ag$^-$g* | 12.0 | 12.6 | 0.5 | 13.8 | 11.4 | 0.6 | 13.3 | 9.6 | 0.7 |
| *tc-Aaa* | 21.7 | 24.2 | <0.1 | 23.1 | 22.9 | <0.1 | 26.1 | 21.2 | <0.1 |
| **tc-Ggg* | 28.8 | 35.3 | <0.1 | 27.2 | 31.4 | <0.1 | 29.8 | 28.8 | <0.1 |
| **tc-Gga* | 29.1 | 34.6 | <0.1 | 28.2 | 31.3 | <0.1 | 28.1 | 28.8 | <0.1 |
| **tc-Ag$^-$a* | 28.7 | 32.0 | <0.1 | 30.1 | 30.4 | <0.1 | 31.4 | 29.0 | <0.1 |
| **cc-Gag* | 36.2 | 44.7 | <0.1 | 34.1 | 39.8 | <0.1 | 40. | 41.8 | <0.1 |
| *cc-Aaa* | 42.8 | 45.9 | <0.1 | 43.7 | 43.9 | <0.1 | 47.4 | 43.7 | <0.1 |

linked to the OCCC dihedral angles is a stabilizing factor: **tt-G**a**a* is more stable than **tt-Gg**g**a*, **tt-Gg**a*** than **tt-Gg**g*** (difference highlighted in bold).

The *tc* family is composed of 9 structures, lying between 11 and ∼30 kJ/mol above the global minimum. The **tc-Gag* conformer is the lowest in energy in the *tc* family at 11.9 kJ/mol. The other conformers are *tc-Aaa*, **tc-Gga*, **tc-Ggg*, **tc-Aga*. The stabilization of **tc-Gag* is explained by the presence of an internal C=O···HO hydrogen bond (d=1.833 Å, $\widehat{OHO}$=155.9°) enabled by the *trans* and *cis* orientation of the two carboxyl groups. It brings 2 kJ/mol in stability compared to the highest-energy *tt*-conformer *tt-Agg*, and 11 kJ/mol compared to the next *tc*-conformer *tc-Aaa* lying at 23.1 kJ/mol (see Table I). The **tc-Ggg* form at 27.2 kJ/mol also presents an internal hydrogen bond linking the two OH groups of the carboxyl ends (d=1.938 Å, $\widehat{OHO}$=150.8°). It is weaker than the hydrogen bond encountered in **tc-Gag* and it cannot compensate the stability loss caused by the constraints on the skeleton in **tc-Ggg*, explaining its higher energy at 27.2 kJ/mol.

Only three conformers have been found in the *cc*-family. The **cc-Gag* conformer and its mirror image are at 34.1 kJ/mol. Similar to **tc-Gag*, it possesses an internal hydrogen bond (d=1.830 Å, $\widehat{OHO}$=155.2°) but displays two *cis*-carboxyl groups instead of one *trans* and one *cis* for the former. The *trans* to *cis* rotation costs 22.2 kJ/mol in energy due to the loss of the stabilizing close contact between the C=O and OH groups, existing only in a *trans*-carboxyl. The highest-energy conformer *cc-Aaa* at 43.7 kJ/mol is linear. It resembles the *tt-Aaa* conformer but with two *cis*-carboxyl groups. It is destabilized by more than 40.0 kJ/mol compared to *tt-Aaa*.

As already mentioned, the *tt*-conformers are in general the most stable forms at the DFT and MP2 level of theory however, the energetic ordering slightly differs depending on the method used, as was reported by Jahn et al.[20]. For instance, the hydrogen-bonded conformer **tc-Gag* is stabilized with DFT-D3BJ at 11.9 kJ/mol at the expense of **tt-Ag$^-$g$^-$* and *tt-Ag$^-$g* at 12.83 and 13.8 kJ/mol, respectively. On the contrary, it is less stable than these two *tt*-conformers and increases at 17.3 kJ/mol with MP2. A stability inversion is also observed between **tc-Ggg* and **tc-Gga*. It is also worth noticing that the ordering is very different with B3LYP without dispersion correction, even though the *tt*-forms are the lowest in energy. That **tt-Gaa* and *tt-Aaa* are isoenergetic without the correction is the most peculiar example.

We have also estimated the conformers' abundances at 298 K from the relative Gibbs free energies assuming a Boltzmann distribution (see Table I). The double degeneracy due to the symmetric forms has been taken into account in calculating the relative populations. The four lowest energy conformers and their symmetric forms account for 98% of the population at 298 K with B3LYP-D3BJ (97% with MP2). The dispersion correction causes no effect on the relative stability at 298 K and the ordering is similar at the two DFT levels (**tt-Gaa* < *tt-Aaa* < **tt-Gga* < **tt-Aga*). The changes are more significant at the MP2 level and we notice a stability inversion between the two most stable conformers: **tt-Gaa* is destabilized by 3.3 kJ/mol compared to *tt-Aaa* with D3BJ, whereas the latter is higher in energy by 1.3 kJ/mol with MP2 (see Table I). We deduce the relative abundance of the four lowest-energy conformers: ∼32:59:4:3 with DFT-D3BJ vs. ∼66:19:6:6 with MP2, i.e. the population of **tt-Gaa* represents 32% at the D3BJ level and increases to 66% when using MP2 (respectively 59% and 19% for *tt-Aaa*). MP2 is known to overbind non-covalent interactions. Recent tests of the MP2 method (and its modifications) on benchmark data including hydrogen-bonding complexes have reported an RMSD of almost 2 kJ/mol, which is slightly better than the B3LYP-D3BJ method (2.5 kJ/mol)[38]. These errors are of the same order of magnitude as the Gibbs free energy difference between the two conformers, which makes any conclusion on the stability inversion difficult.

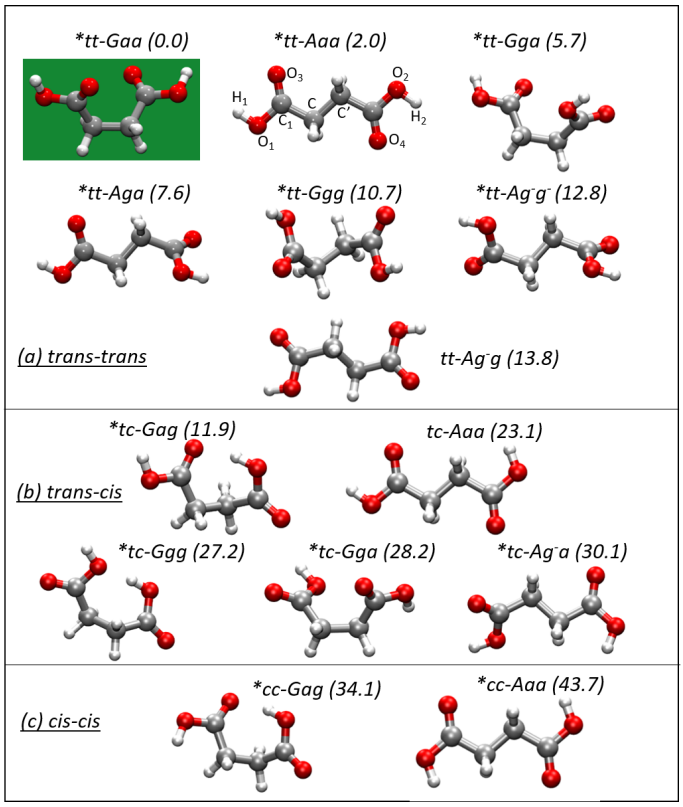


FIG. 1. Conformers of succinic acid optimized at the B3LYP-D3BJ/6-311++G(d,p) level of theory: (a) *trans-trans* configuration of the carboxyl groups, (b) *trans-cis*, (c) *cis-cis*. The conformers presenting a symmetrical form are marked with an asterisk. The most stable **tt-Gaa* form is emphasized by a different color background.

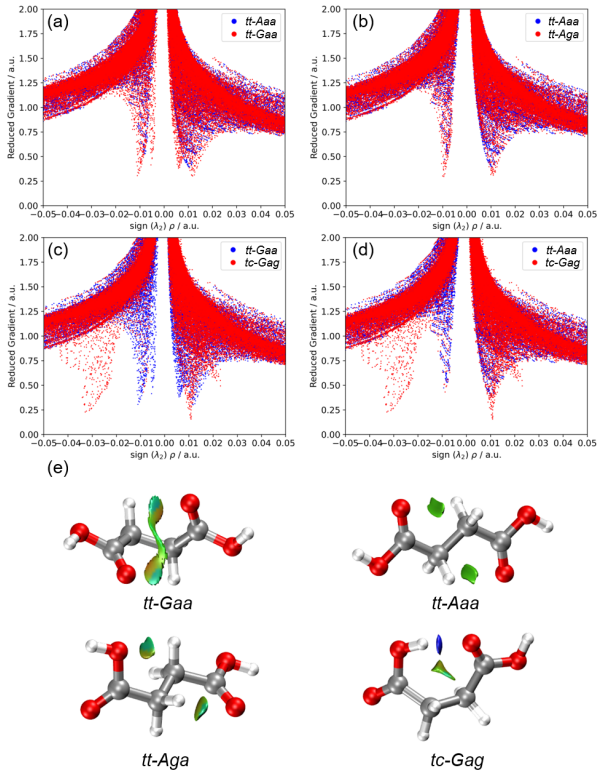


FIG. 2. NCI plots of the *tt-Gaa*, *tt-Aaa*, *tt-Aga*, and *tc-Gag* conformers calculated at the B3LYP-D3BJ level of theory.

## B. NCI analysis

We have conducted NCI calculations to help understand the nature of the interactions at play in the relative stability of the conformers. They have been carried out on the most relevant conformers of succinic acid, mostly on the *tt*-conformers for are the lowest-energy species, and on representative *tc* and *cc*-conformers. Figure 2 shows the reduced density gradient together with the favorable NCI gradient isosurfaces of the four lowest-energy conformers, represented with an isovalue of 0.6 a.u. We compare one conformer with another using two colors (in contrast with other common plots displaying a three-color code). The negative sign of the eigenvalue refers to stabilizing interaction, the more negative, the stronger the interaction. The positive sign refers to repulsive interactions.

The NCI analysis indicates the presence of weak stabilizing CH···O interactions between the ethyl group and the oxygen atom from the carbonyl or the hydroxyl group. They are represented as green-colored surfaces in all conformers in Figure 2e. Blue surfaces, indicative of stronger interactions are only visible for the conformers with an intramolecular hydrogen bond, such as **tc-Gag*. Figure 2a compares the results obtained for the two most stable forms, the *gauche* **tt-Gaa* and the linear *tt-Aaa* (red and blue, respectively). The common spike in the $\lambda_2$ negative sign pertains to CH···O interactions. They are present in the two conformers but they are stronger in the case of **tt-Gaa*. The latter bears an additional stabilization, weaker than the CH···O, that is reflected by the delocalized surface (see Figure 2e). The two linear structures *tt-Aaa* and **tt-Aga* show very similar NCI plots (see Figure 2b), which do not explain the 5.6 kJ/mol energy difference between the two structures. The difference in the reduced density gradient is more striking with the **tc-Gag-* conformer. In Figure 2c and d, the main difference between **tc-Gag* and *tt-Gaa* or *tt-Aaa* is the intense dip at -0.03 a.u., which is an indicator of the internal hydrogen bond between the two carboxyl groups in **tc-Gag*.

Looking more carefully at the NCI analysis, we notice that the results are not able to reproduce the subtle effects responsible for the stabilization of the conformers of succinic acid. It appears that the linear conformers display very similar plots. The same is true for *gauche* conformers or those with an internal hydrogen bond. The NCI analysis can only reveal the main interactions involving the carbon backbone independent of the orientation of the carboxyl ends of the acid. It is illustrated in Figure 3 by the NCI plots of the four linear conformers *tt-Aaa*, **tt-Aga*, *tc-Aaa*, and **cc-Aaa*, exhibiting common spikes in the positive or the negative part of the graph. A similar result is obtained for the folded forms **tt-Gaa*, **tt-Gga*, **tt-Ggg*, and **tc-Gga* (see Figure S2(a) in SM), indicating that the NCI analysis is non-specific. The comparison for the hydrogen-bonded conformers **tc-Gag*, **cc-Gag*, and **tc-Ggg* is also

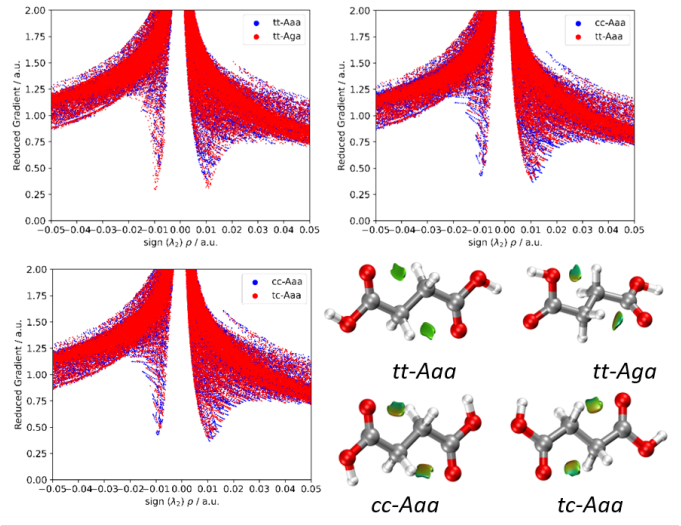


FIG. 3. NCI plots of the linear conformers *tt-Aaa*, *tt-Aga*, *cc-Aaa*, *tc-Aaa* calculated at the B3LYP-D3BJ level of theory.

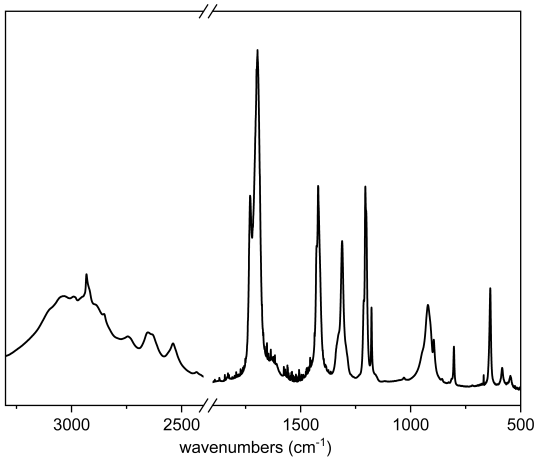


FIG. 4. IR spectrum of succinic acid in a KBr pellet (1:1000 mass ratio) in the mid-IR region.

very interesting (see Figure S2(b) in SM). The large dip at -0.03 a.u. reproduces the strong OH···C=O hydrogen bond quite well for the two *Gag* forms (hydrogen-bond distance of about 1.830 Å, $\nu$OH predicted at 3360 and 3368 cm$^{-1}$, see Table S2 in SM) but the NCI analysis gives no hints regarding the 22 kJ/mol difference between them. It means that the stabilization linked to *trans*-carboxyl group in **tc-Gag*, and in general, is not considered at all in the NCI approach. As to the hydrogen-bonded **tc-Ggg* conformer, the NCI plot reproduces the weaker OH···OH hydrogen bond between the two hydroxyl groups (dip at -0.025 a.u. instead of -0.03 a.u. for the OH···C=O). That the theoretical $\nu$OH mode is blue-shifted to 3496 cm$^{-1}$ is also an indicator of a looser hydrogen bond.

Our global theoretical approach agrees with Jahn et al.[20] but brings a deeper understanding of the factors dictating the energetic ordering. The increased stability of the folded **tt-Gaa* over the linear *tt-Aaa* was attributed to the *gauche effect*[20]. We also observe a similar trend when the carbon backbone adopts a *gauche* configuration (*first letter G*), making it more stable than its *anti* counterpart (first letter *A*): E(*tt-**G**ga*)< E(*tt-**A**ga*), E(*tt-**G**gg*)<E(*tt-**A**gg*), E(*tc-**G**ga*)<E(*tc-**A**ga*), etc. Conversely, the *gauche* conformation of the O(H)CCC dihedral angle induces steric hindrance between the carboxyl oxygen (C=O) and the adjacent hydrogen (distance <2.60 Å), destabilizing the *gauche* form over the *anti*. Hence the energetic stability of the conformers of succinic acid is dictated by multiple factors, the *G/A* arrangement of the carbon skeleton; the OH···O=C interactions within the carboxyl groups resulting in the *tt*-conformers being lower in energy; CH···O interactions, also known as "CH bonds". The latter interactions and hydrogen bonds have been identified in the NCI analysis but the method fails to reproduce the stabilizing effects of the OH···C=O close contacts within the carboxyl groups, neither can it explain the stability of the two most stable conformers *tt-Gaa* and *tt-Aaa* since they do not exhibit specific NCI plots.

### C. Solid state spectrum

The solid-state spectra of succinic acid have been measured in the mid-IR region at room temperature. The broad bands in the 3000 cm$^{-1}$ region are the signatures of hydrogen-bonded OH vibrations. They are overlapped with the CH stretching bands (2700-2900 cm$^{-1}$), which are less intense (Figure 4). The bands in the fingerprint region (1800-500 cm$^{-1}$) pertain to the vibrational modes of the carboxyl groups and the carbon skeleton (stretch, bend, torsion, etc.). The additional bands near 2600 cm$^{-1}$ belong to combination bands. The spectrum is quite similar to the results reported in the literature[9,13,39], assigning the IR signature to the $\beta$-polymorph of succinic acid[11,13]. The $\beta$-form consists of hydrogen-bonded chains of succinic acids, each acidic unit adopting a planar skeleton (CCCC dihedral angle about 180°). The carboxyl groups are *anti* (HOCC dihedral angle about 180°) and are twisted by approximately 11° from the skeletal plane[9,11] (O(H)CCC dihedral angle of 11°). Our conformational search in the gas phase did not succeed in finding the 11°-twisted structure. The planar *tt-Aaa* conformer is the closest to this twisted structure but differs by coplanar skeleton and carboxyl groups. We have built on *tt-Aaa* to construct a planar dimeric structure of succinic acid[11,13], labeled D1. A cyclic dimer, labeled D2, has also been considered for comparison. 9 other monomers also adopt an *anti*-configuration of the carbon skeleton (180°), **tt-Aga*, **tt-Ag-g-*, *tt-Ag-g*, *tc-Aaa*, **tc-Ag-a*, *cc-Aaa* (see Figure S3 in SM). We have performed geometry and frequency calculations on these linear structures and compared them with the IR spectrum in KBr. We note that several bands can only be reproduced by the calculations of D1 planar dimer, such as the red-shifted C=O stretch near 1695 cm$^{-1}$ and the band near 920 cm$^{-1}$, respectively the symmetric C=O stretch and in-phase out-of-plane OH bend (Figure 5). In particular, neither the cyclic D2 dimer nor the linear *tt-Aaa* monomer give a good match with the spectrum in KBr (see Figure S4 and S5 in SM). Our analysis is in favor of the D1 planar dimer structure being responsible for the IR spectrum.

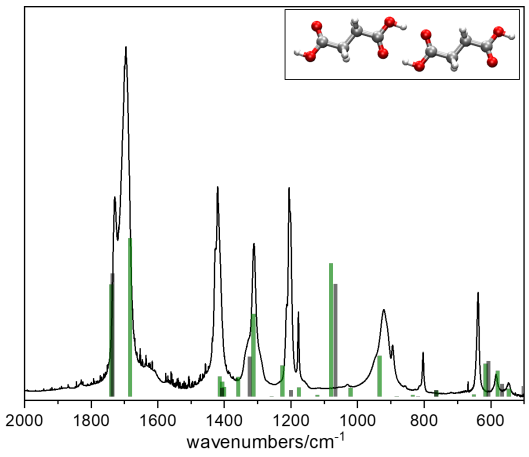


FIG. 5. Comparison between the IR spectrum of succinic acid in KBr with the theoretical frequencies of the D1 planar dimer and the *tt-Aaa* conformer calculated at the B3LYP-D3BJ/6-311++G(d,p) level of theory, shown as column bars (respectively in green and gray). The frequencies are scaled with different factors depending on the region, but they are kept the same for both species, see text.

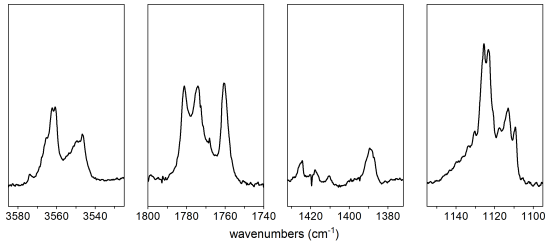


FIG. 6. Mid-IR spectrum of succinic acid in argon at 20K in selected regions.

The non-symmetrical shape of the bands at 1695, 1310, and 920 cm$^{-1}$ indicates the possible presence of more than one species in KBr. Tentative attribution based on the energetics solely would be too simplistic since (i) our calculations have been done in the gas phase and not in the solid phase, (ii) the constraints encountered in the solid state would likely favor some conformers that have been found at higher energy in the gas phase. A more precise assignment of these bands will thus not be addressed here. In any case, results clearly indicate that an extended planar structure is favored in the solid state.

### D. IR spectrum in argon matrix

The IR spectrum of succinic acid isolated in argon at 20 K in selected regions is presented in Figure 6. The most intense bands are seen in the OH, C=O, and CO stretching regions near 3550, 1760, and 1120 cm$^{-1}$, respectively, consisting of multiplet-band structures, which are due to different trapping sites in the argon matrix: 1781.1/1774.2, 1125.6/1123.1. The weaker bands around 1400 cm$^{-1}$ are assigned to CH stretch modes.

TABLE II. Frequencies of the vibrational modes of succinic acid observed in KBr and in argon at 20 K (most intense bands) and theoretical frequencies for D1 planar dimer and **tt-Gaa* conformer calculated at the B3LYP-3DBJ/6-311++G(d,p). Frequencies are scaled (see Computational methods for the scaling factors).

| | KBr pellet | | | Argon matrix | |
|---|---|---|---|---|---|
| Exp. | D1 Planar | D2 Cyclic | Assignment[a] | Exp.[c] | Monomer **tt-Gaa* |
| 3450 | 3400 (148) | | $\nu$OH | 3561.9 | 3552 (77) |
| | | | | 3550.8 | 3552 (65) |
| | | | | 3546.7 | |
| 2932 | 2939 (3608) | 3129 (2558) | $\nu$OH | | |
| | | 3109 (29) | | | |
| | | 3079 (21) | | | |
| 3045 | 3005 (8) | 3045 (7) | | 2978 *br* | |
| 2989 | 2987 (29) | 2972 (13) | $\nu CH_{as}$ | 2935 *br* | 2940 (3) |
| | | | | 2886 *br* | 2883 (12) |
| 2744 | | | FR[b] | n/o | |
| 2656 | | | FR[b] | n/o | |
| 2540 | | | FR[b] | n/o | |
| 1729 | 1738 (568) | 1700 (1008) | $\nu$C=O | 1781.0 *s* | |
| | | | | 1774.4 | 1771 (150) |
| 1695 | 1682 (801) | 1683 (118) | | 1760.3 *s* | 1766 (448) |
| | | 1662 (74) | | | |
| 1421 | 1412 (103) | 1424 (126) | $\delta$OH$\cdots$O | 1424.4 | |
| | 1405 (76) | 1410 (14) | | 1417.8 | 1419 (22) |
| | 1399 (50) | 1380 (99) | $\omega CH_2$ | 1410.6 | 1415 (22) |
| | 1357 (101) | 1377 (40) | | 1389.6 | 1373 (119) |
| | | | | 1365.2 | |
| 1311 | 1311 (419) | 1307 (32) | $\nu$CO | n/o | |
| | 1256 (2) | 1298 (69) | | 1278.0 | |
| 1206 | 1224 (159) | 1195 (191) | | 1207.0 | 1229 (4) |
| | | 1192 (100) | | | |
| 1178 | 1174 (48) | 1188 (249) | $\tau CH_2$ | 1125.7 | 1118 (559) |
| | | 1148 (18) | | 1113.2 | |
| 1030 | 1119 (9) | 1115 (164) | | n/o | |
| 1030 | 1078 (676) | 1109 (42) | | | |
| 921 | 932 (208) | 922 (4) | | 952.8 | 942 (14) |
| 895 | 880 (3) | | | n/o | |
| 804 | 832 (9) | 806 (204) | | 800.6 | 805 (18) |
| | 761 (32) | 772 (223) | | | |
| | | 769 (286) | | | |
| | | 756 (45) | | | |
| 638 | 648 (13) | 659 (41) | | n/o | |
| 584 | 577 (132) | 568 (23) | | n/o | |
| 547 | 543 (40) | 547 (19) | | n/o | |

[a] From Suzuki et al. [13]
[b] Fermi resonance.
[c] s: strong, br: broad.

The assignment of the IR bands has been guided by the computational results. Different scaling factors have been applied to the vibrational modes, they have been kept constant for all conformers of the three *tt*, *tc*, and *cc* families: 0.945 above and 0.975 below 3200 cm$^{-1}$. Among the 24 conformers computed, the *tt*-forms give a satisfactory agreement and overall, the most intense bands are correctly reproduced. We

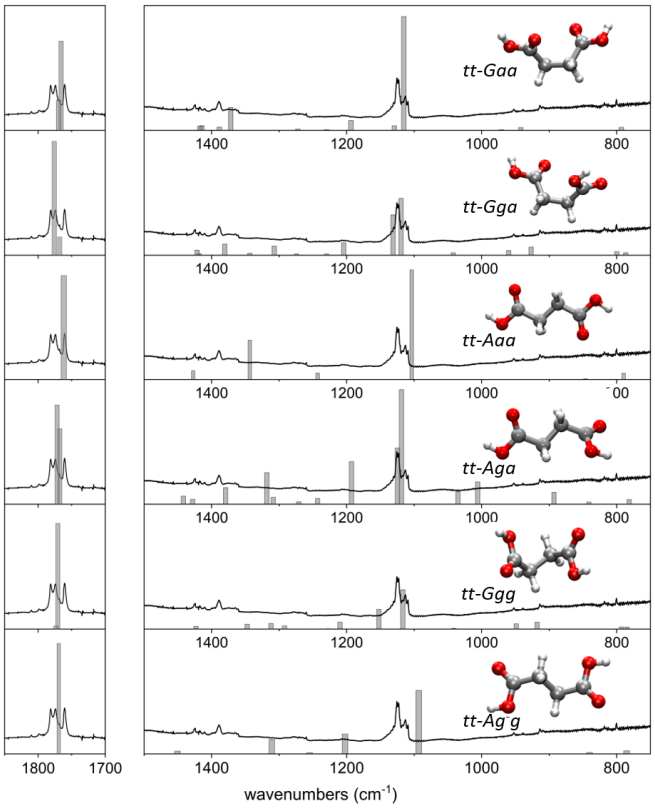


FIG. 7. IR spectrum of succinic acid in argon compared with the computed frequencies of *tt-*Gaa* (a), *tt-Gga* (b) and *tt-Aaa* (c) shown as stick spectra, at the B3LYP-D3BJ/6-311++G(d,p) level of theory.

have discarded the *tc* and *cc*-conformers based on the mismatch in the OH stretch and C=O stretch regions (see Figure S6 in the Supplementary Material). They are also very high in energy (Table I). A very good agreement is obtained for the most stable *tt-Gaa* conformer as shown in Figure 7 (top spectrum) and Table II. The experimental OH stretch, C=O stretch, and the CO stretch bands at 3546.7, 1760.3, and 1125.7 $cm^{-1}$ are very well reproduced in terms of position and band intensity. The $\nu$OH and $\nu$C=O bands absorb at typical frequencies of free *trans*-carboxyl groups, where neither C=O nor OH is involved in hydrogen bonds, in argon matrices, i.e. above 3540 $cm^{-1}$ for $\nu$OH and at 1740-1790 $cm^{-1}$ for $\nu$C=O. The vibrational modes of free *cis*-carboxyl groups typically absorb at higher frequencies[34,40–43]. We cannot assign all the experimental bands to *tt-*Gaa* since all the multiplet band structures are not solely due to matrix site effects. Succinic acid has been heated up to 355 K, allowing several conformers to be populated, at least the most stable ones. The vibrational spectrum may thus reflect the contribution of additional conformers. In particular, the $\nu$OH and $\nu$CO bands are rather broad and the components of the $\nu$OH and $\nu$C=O multiplets are separated by $\sim$14 $cm^{-1}$, which we interpret as being due to other conformers. Based on the same argument as for the *tt-*Gaa* bands, we attribute the unassigned bands in the $\nu$OH and $\nu$C=O region to *tt*-conformers. This rationale gives an explanation for the good match between the calculated frequencies of the *tt*-conformers and experiments as noticed previously. It also enables us to narrow the list of plausible candidates to the *tt*-forms only. The populations at 298 K of the four lowest conformers have already been given in a previous section: *tt-*Gaa* accounts for 32%, *tt-Aaa* for 59%, *tt-*Ggg* for 4%, and *tt-*Aga* for 3%, the remaining conformers accounting for less than 2%. Therefore, we expect *tt-Aaa* to contribute significantly to the IR spectrum of succinic acid in argon. We recall that this conformer resembles the planar dimer in the KBr studies and that it was reported in aqueous solution[22,23]. The theoretical frequencies of *tt-Aaa* give a satisfactory match with the spectrum but it is not the predominant form, which is the most stable *tt-*Gaa*[19,20]. Another good candidate is *tt-*Gga* of which frequencies fit quite well with the experiment (Figure 7). However, its contribution should be very low (abundance of 4%). We can discard the fourth structure, *tt-*Aga* because of its low population (3%) and its higher relative energy (7.6 kJ/mol). Hence, the IR spectrum very likely reflects the contribution of different conformers of succinic acid.

## V. CONCLUSION

The vibrational spectra of succinic acid have been measured in a KBr pellet and an argon matrix at cryogenic temperatures by IR spectroscopy. Guided by quantum calculations we have characterized the structural properties of the acid. The theoretical frequencies of succinic acid dimer with a planar geometry reproduce satisfactorily the IR spectrum in KBr. We hypothesize the presence of other conformers (dimer-like or monomers) but further computational approaches are required for a better description of the packing effects at play in the solid state, which we do not mean to address in this article. The vibrational signature of the most stable *gauche* conformer *tt-*Gaa* has been evidenced here in matrix isolation measurements. We have also observed additional IR signatures that are assigned to other *tt*-conformers of succinic acid. The linear *tt-Aaa* form may contribute to the experimental spectrum, although at a low amount, and therefore cannot be ruled out due to experimental limitations. That the populations obtained by the free Gibbs energy are not manifested experimentally may be caused by the matrix conditions, which do not reproduce a Boltzmann equilibrium. A better description of the mechanisms at play from the vaporization of succinic acid to the trapping in the matrix would yield an accurate interplay between energy and free Gibbs energy, but it is beyond the scope of this study. While rotational spectroscopy is sensitive to the value of the permanent dipole moment, IR spectroscopy can circumvent the lack of, or low permanent dipole moment, explaining the presence of a mixture of conformers in the cryogenic matrix. Our assumption is in line with liquid-phase and gas electron diffraction studies reporting the co-existence of extended-like conformers and *gauche*-structures.

We have provided a complete picture of the conformational landscape of succinic acid and we have tentatively identified the stabilizing factors responsible for the energetic ordering of the conformers. The interplay between hydrogen bonds and

weaker non-covalent interactions is not the determining factor for governing the stability of succinic acid, although it is commonly the case for other systems. Yet it influences the ordering of the higher energy conformations. These interactions have to compete with the torsion of the backbone that stabilizes the *gauche* geometry, making it the most stable form. Non-covalent interactions have been analyzed and identified in the NCI analysis but this approach does not reproduce more subtle effects such as the OH$\cdots$C=O close contacts within the carboxyl groups, responsible for the increased stability of the *tt*-conformers.

Identifying the most populated structures in the gas phase is crucial. The propensity for succinic acid to adopt an extended-like or folded structure may influence its aggregation process toward the formation of large particles. It can also have an impact on the wetting properties of small dicarbonyl pollutants since their hygroscopicity may depend on the conformation. Additionally, in an atmospheric simulation chamber, the secondary organic aerosols formed by the reaction with major nucleating precursors ($O_3$, $H_2SO_4$, $NO_3^-$, OH, etc.) are often characterized by measuring samples collected on filters by ATR (Attenuated Total Reflectance) IR spectroscopy. In particular, the spectra in the fingerprint region allow the identification of their molecular composition. Therefore, the data recorded in the present study might be useful to detect the presence, or the absence thereof, of succinic acid in such samples of secondary organic aerosols.

## SUPPLEMENTARY MATERIAL

Fig. S1: Newmann projection of the conformers of succinic acid.

Fig. S2: NCI plots of selected conformers of succinic acid: (a) *gauche G*-conformers, (b) conformers with an internal hydrogen bond, (c) corresponding structures.

Fig. S3: Calculated structures of the linear forms of succinic acid and two dimers: D1 is a planar dimer, D2 is a cyclic dimer.

Fig. S4: IR spectrum of succinic acid in KBr compared with the scaled theoretical frequencies of D1 planar dimer and D2 cyclic dimer.

Fig. S5: Comparison of the calculated IR spectra of the D1 planar dimer and the *tt-Aaa* conformer. The frequencies have been scaled and have been convoluted with a Lorentzian profile of 10 $cm^{-1}$ full-width-half-maximum.

Fig. S6: IR spectrum of succinic acid in argon at 20 K compared with the theoretical frequencies of selected *tc*-conformers and *cc*-conformers, shown as stick spectra.

Table S1: Geometrical parameters of selected *tt*-conformers of succinic acid ($<$14 kJ/mol).

Table S2: Theoretical frequencies and relative energies corrected for ZPE of selected *tt*, *tc* and *cc*-conformers of succinic acid.

Table S3: Cartesian coordinates of the conformers of succinic acic.

## ACKNOWLEDGEMENTS

This work was supported by the ANR DYNAAMIX project (ANR-17-CE29-0001-01) of the French National Research Agency (ANR). AC fellowship was supported by Investissements d'Avenir du LabEx PALM (ANR-10-LABX-0039-PALM). The authors (JAC and MG) acknowledge the CaPPA project and the CPER ECRIN funded by the ANR through the PIA 11-LABX-0005-01, the I-SITE ULNE/ANR-16-IDEX-0004 ULNE, the Regional Council Hauts-de-France and the European Funds for Regional Economic Development (FEDER). This work was performed using the computational resources from the "Mésocentre" computing center of Centrale Supélec and École Normale Supérieure Paris-Saclay supported by CNRS and Région Ile-de-France (`https://mesocentre.centralesupelec.fr/`).

The authors declare no conflict of interest.

[1] A. Chebbi and P. Carlier, "Carboxylic acids in the troposphere, occurrence, sources, and sinks: A review," Atmos. Environ. **30**, 4233 – 4249 (1996).

[2] S. K. R. Boreddy, P. Hegde, and A. R. Aswini, "Summertime high abundances of succinic, citric, and glyoxylic acids in antarctic aerosols: Implications to secondary organic aerosol formation," J. Geophys. Res.: Atmospheres **127**, e2021JD036172 (2022).

[3] J. Lightstone, T. Onasch, and D. Imre, "Deliquescence, efflorescence, and water activity in ammonium nitrate and mixed ammonium nitrate/succinic acid microparticles," J. Phys. Chem. A **104**, 9337–9346 (2000).

[4] W. Xu and R. Zhang, "Theoretical investigation of interaction of dicarboxylic acids with common aerosol nucleation precursors," J. Phys. Chem. A **116**, 4539–4550 (2012).

[5] T. Yli-Juuti, A. A. Zardini, A. C. Eriksson, A. M. K. Hansen, J. H. Pagels, E. Swietlicki, B. Svenningsson, M. Glasius, D. R. Worsnop, I. Riipinen, and M. Bilde, "Volatility of organic aerosol: Evaporation of ammonium sulfate/succinic acid aqueous solution droplets," Environ. Sci. Technol. **47**, 12123–12130 (2013).

[6] R. Zhang, I. Suh, J. Zhao, D. Zhang, E. C. Fortner, X. Tie, L. T. Molina, and M. J. Molina, "Atmospheric new particle formation enhanced by organic acids," Science **304**, 1487–1490 (2004).

[7] M. Kulmala, J. Kontkanen, H. Junninen, K. Lehtipalo, H. E. Manninen, T. Nieminen, T. Petäjä, M. Sipilä, S. Schobesberger, P. Rantala, A. Franchin, T. Jokinen, E. Järvinen, M. Äijälä, J. Kangasluoma, J. Hakala, P. P. Aalto, P. Paasonen, J. Mikkilä, J. Vanhanen, J. Aalto, H. Hakola, U. Makkonen, T. Ruuskanen, R. L. Mauldin, J. Duplissy, H. Vehkamäki, J. Bäck, A. Kortelainen, I. Riipinen, T. Kurtén, M. V. Johnston, J. N. Smith, M. Ehn, T. F. Mentel, K. E. J. Lehtinen, A. Laaksonen, V.-M. Kerminen, and D. R. Worsnop, "Direct observations of atmospheric aerosol nucleation," Science **339**, 943–946 (2013).

[8] R. Zhang, G. Wang, S. Guo, M. Zamora, Q. Ying, Y. Lin, W. Wang, M. Hu, and Y. Wang, "Formation of urban fine particulate matter," Chem. Rev. **115**, 3803–3855 (2015).

[9] L. A. Duncanson, "A study of the variations produced by sublimation in the infra-red spectra of some substituted succinic acids," J. Chem. Soc. , 1753–1761 (1952).

[10] G. D. Buckley, "Supposed rotational isomerism in the succinic acid series," J. Chem. Soc. , 1325–1328 (1953).

[11] J. S. Broadley, D. W. J. Cruickshank, J. D. Morrison, J. M. Robertson, and H. M. M. Shearer, "Three-dimensional refinement of the structure of $\beta$-succinic acid," Proc. R. Soc. Lond. A **251**, 441–457 (1959).

[12] G. D. Rieck, "The crystal structure of $\alpha$-succinic acid," Recueil des Travaux Chimiques des Pays-Bas **63**, 170–180 (1944).

[13] M. Suzuki and T. Shimanouchi, "Infrared and raman spectra of succinic acid crystal," J. Molec. Spectry **28**, 394–410 (1968).

[14] H. T. Flakus, B. Hachuła, and J. T. Hołaj-Krzak, "Long-distance inter-hydrogen bond coupling effects in the polarized ir spectra of succinic acid crystals," Spectrochim. Acta A **142**, 126–134 (2015).

[15] V. Pokorný, P. Touš, V. Štejfa, K. Růžička, J. Rohlíček, J. Czernek, J. Brus, and C. Červinka, "Anisotropy, segmental dynamics and polymorphism of crystalline biogenic carboxylic acids," Phys. Chem. Chem. Phys. **24**, 25904–25917 (2022).

[16] T. J. McMahon, J. R. Bailey, and R. G. Bird, "Structure and dynamics of succinic, methylsuccinic and itaconic anhydrides in the gas phase," J. Molec. Spectry **347**, 35–40 (2018).

[17] M. K. Jahn, D. A. Obenchain, K. P. R. Nair, J.-U. Grabow, N. Vogt, J. Demaison, P. D. Godfrey, and D. McNaughton, "The puzzling hyper-fine structure and an accurate equilibrium geometry of succinic anhydride," Phys. Chem. Chem. Phys. **22**, 5170–5177 (2020).

[18] Y. Lin, Y. Ji, Y. Li, J. Secrest, W. Xu, F. Xu, Y. Wang, T. An, and R. Zhang, "Interaction between succinic acid and sulfuric acid–base clusters," Atmos. Chem. Phys., **19**, 8003–8019 (2019).

[19] N. Vogt, M. A. Abaev, A. N. Rykov, and I. F. Shishkov, "Determination of molecular structure of succinic acid in a very complex conformational landscape: Gas-phase electron diffraction (ged) and ab initio studies," J. Mol. Struct. **996**, 120–127 (2011).

[20] M. K. Jahn, E. Méndez, K. P. Rajappan Nair, P. D. Godfrey, D. McNaughton, P. Écija, F. J. Basterretxea, E. J. Cocinero, and J.-U. Grabow, "Conformational steering in dicarboxy acids: the native structure of succinic acid," Phys. Chem. Chem. Phys. **17**, 19726–19734 (2015).

[21] J. D. Roberts, "Fascination with the conformational analysis of succinic acid, as evaluated by nmr spectroscopy, and why," Acc. Chem. Res. **39**, 889–896 (2006).

[22] J. Werner, J. Julin, M. Dalirian, N. L. Prisle, G. Öhrwall, I. Persson, O. Björneholm, and I. Riipinen, "Succinic acid in aqueous solution: connecting microscopic surface composition and macroscopic surface tension," Phys. Chem. Chem. Phys. **16**, 21486–21495 (2014).

[23] P. G. Blower, S. T. Ota, N. A. Valley, S. R. Wood, and G. L. Richmond, "Sink or surf: Atmospheric implications for succinic acid at aqueous surfaces," J. Phys. Chem. A **117**, 7887–7903 (2013).

[24] R. Pollet and W. Chin, "Reversible hydration of $\alpha$-dicarbonyl compounds from ab initio metadynamics simulations: Comparison between pyruvic and glyoxylic acids in aqueous solutions," J. Phys. Chem. B **125**, 2942–2951 (2021).

[25] W. Chin, M. Chevalier, R. Thon, R. Pollet, J. Ceponkus, and C. Crépin, "Photochemistry of glycolaldehyde in cryogenic matrices," The Journal of Chemical Physics **140**, 224319 (2014).

[26] P. Pracht, F. Bohle, and S. Grimme, "Automated exploration of the low-energy chemical space with fast quantum chemical methods," Phys. Chem. Chem. Phys. **22**, 7169–7192 (2020).

[27] S. Grimme, "Exploration of chemical compound, conformer, and reaction space with meta-dynamics simulations based on tight-binding quantum chemical calculations," J. Chem. Theory Comput. **15**, 2847–2862 (2019).

[28] C. Bannwarth, S. Ehlert, and S. Grimme, "Gfn2-xtb—an accurate and broadly parametrized self-consistent tight-binding quantum chemical method with multipole electrostatics and density-dependent dispersion contributions," J. Chem. Theory Comput. **15**, 1652–1671 (2019).

[29] S. Grimme, S. Ehrlich, and L. Goerigk, "Effect of the damping function in dispersion corrected density functional theory," J. Comput. Chem. **32**, 1456–1465 (2011).

[30] M. J. Frisch, G. W. Trucks, H. B. Schlegel, G. E. Scuseria, M. A. Robb, J. R. Cheeseman, G. Scalmani, V. Barone, G. A. Petersson, H. Nakatsuji, X. Li, M. Caricato, A. V. Marenich, J. Bloino, B. G. Janesko, R. Gomperts, B. Mennucci, H. P. Hratchian, J. V. Ortiz, A. F. Izmaylov, J. L. Sonnenberg, D. Williams-Young, F. Ding, F. Lipparini, F. Egidi, J. Goings, B. Peng, A. Petrone, T. Henderson, D. Ranasinghe, V. G. Zakrzewski, J. Gao, N. Rega, G. Zheng, W. Liang, M. Hada, M. Ehara, K. Toyota, R. Fukuda, J. Hasegawa, M. Ishida, T. Nakajima, Y. Honda, O. Kitao, H. Nakai, T. Vreven, K. Throssell, J. A. Montgomery, Jr., J. E. Peralta, F. Ogliaro, M. J. Bearpark, J. J. Heyd, E. N. Brothers, K. N. Kudin, V. N. Staroverov, T. A. Keith, R. Kobayashi, J. Normand, K. Raghavachari, A. P. Rendell, J. C. Burant, S. S. Iyengar, J. Tomasi, M. Cossi, J. M. Millam, M. Klene, C. Adamo, R. Cammi, J. W. Ochterski, R. L. Martin, K. Morokuma, O. Farkas, J. B. Foresman, and D. J. Fox, "Gaussian~16 Revision C.01," (2016), gaussian Inc. Wallingford CT.

[31] W. Humphrey, A. Dalke, and K. Schulten, "VMD – Visual Molecular Dynamics," J. Mol. Graphics **14**, 33–38 (1996).

[32] J. Stone, *An Efficient Library for Parallel Ray Tracing and Animation*, Master's thesis, Computer Science Department, University of Missouri-Rolla (1998).

[33] A.-R. Allouche, "Gabedit—a graphical user interface for computational chemistry softwares," J. Comput. Chem. **32**, 174–182 (2011).

[34] A. Borba, A. Gomez-Zavaglia, L. Lapinski, and R. Fausto, "Rotational isomers of lactic acid: first experimental observation of higher energy forms," Phys. Chem. Chem. Phys. **6**, 2101–2108 (2004).

[35] A. J. Lopes Jesus, C. M. Nunes, I. Reva, S. M. V. Pinto, and R. Fausto, "Effects of entangled ir radiation and tunneling on the conformational interconversion of 2-cyanophenol," J. Phys. Chem. A **123**, 4396–4405 (2019).

[36] E. R. Johnson, S. Keinan, P. Mori-Sánchez, J. Contreras-García, A. J. Cohen, and W. Yang, "Revealing noncovalent interactions," J. Am. Chem. Soc. **132**, 6498–6506 (2010).

[37] J. Contreras-García, E. R. Johnson, S. Keinan, R. Chaudret, J.-P. Piquemal, D. N. Beratan, and W. Yang, "Nciplot: A program for plotting noncovalent interaction regions," J. Chem. Theory Comput. **7**, 625–632 (2011).

[38] M. Loipersberger, L. W. Bertels, J. Lee, and M. Head-Gordon, "Exploring the limits of second- and third-order møller–plesset perturbation theories for noncovalent interactions: Revisiting mp2.5 and assessing the importance of regularization and reference orbitals," J. Chem. Theory Comp. **17**, 5582–5599 (2021), pMID: 34382394.

[39] S. Krishnan, C. J. Raj, R. Robert, A. Ramanand, and S. J. Das, "Growth and characterization of succinic acid single crystals," Cryst. Res. Technol. **42**, 1087–1090 (2007).

[40] E. M. S. Maçôas, R. Fausto, J. Lundell, M. Pettersson, L. Khriachtchev, and M. Räsänen, "Conformational analysis and near-infrared-induced rotamerization of malonic acid in an argon matrix," J. Phys. Chem. A **104**, 11725–11732 (2000).

[41] A. Olbert-Majkut, J. Ahokas, M. Pettersson, and J. Lundell, "Visible light-driven chemistry of oxalic acid in solid argon, probed by raman spectroscopy," J. Phys. Chem. A **117**, 1492–1502 (2013).

[42] A. Olbert-Majkut, J. Lundell, and M. Wierzejewska, "Light-induced opening and closing of the intramolecular hydrogen bond in glyoxylic acid," J. Phys. Chem. A **118**, 350–357 (2014).

[43] I. Reva, C. M. Nunes, M. Biczysko, and R. Fausto, "Conformational switching in pyruvic acid isolated in ar and n2 matrixes: Spectroscopic analysis, anharmonic simulation, and tunneling," J. Phys. Chem. A **119**, 2614–2627 (2015).

[44] P. Lucaioli, E. Nauha, I. Gimondi, L. S. Price, R. Guo, L. Iuzzolino, I. Singh, M. Salvalaglio, S. L. Price, and N. Blagden, "Serendipitous isolation of a disappearing conformational polymorph of succinic acid challenges computational polymorph prediction," Cryst. Eng. Comm. **20**, 3971–3977 (2018).